Chemical Physics 417 (2013) 37–44

Contents lists available at SciVerse ScienceDirect

Chemical Physics

journal homepage: www.elsevier.com/locate/chemphys

Electronic and magnetic properties of 3d transition metal-doped strontium clusters: Prospective magnetic superatoms

Vikas Chauhan, Prasenjit Sen *

Harish-Chandra Research Institute, Chhatnag Road, Jhunsi, Allahabad 211019, India

ARTICLE INFO

Article history:
Received 20 December 2012
In final form 23 March 2013
Available online 1 April 2013

Keywords:
Atomic cluster
Shell model
Magnetic superatom

ABSTRACT

Structural, electronic and magnetic properties of 3d transition metal doped strontium clusters are studied using first-principles electronic structure methods based on density functional theory. Clusters with enhanced kinetic and thermodynamic stability are identified by studying their hardness, second order energy difference and adiabatic spin excitation energy. $CrSr_9$ and $MnSr_{10}$ are found to have enhanced stability. They retain their structural identities in assemblies, and are classified as magnetic superatoms. A qualitative understanding of the magnetic coupling between two cluster units is arrived at. Reactivity of these superatoms with O_2 molecule is also studied. Prospects for using these magnetic superatoms in applications are discussed.

1. Introduction

Atomic clusters have been studied for nearly three decades now, but they are very much in focus even today. Starting with the theoretical work of Ekardt [1] and the pioneering experiments of Knight et al. [2], the so-called electronic shell models have formed a simple conceptual basis for understanding many of the properties of simple metal clusters. The essential idea of all the variants of the shell model [3] is that the (valence) electrons in the clusters are confined in a finite volume. This quantum confinement leads to discrete energy levels, and the symmetry of the confining potential leads to degeneracies. In particular, in a hard sphere confining potential (or a spherical jellium model for interacting electrons), the electronic states bunch into 1S, 1P, 1D, 2S, 1F, 2P, ... shells. Completely filled electronic shells are obtained for 2, 8, 18, 20, 34, 40, ... valence electrons. If the number of valence electrons in a cluster happens to coincide with one of these numbers, a filled electronic shell results, leading to enhanced stability of that cluster (called magic clusters). This simple idea explains most major observations of Knight et al. in the abundance spectra of Na clusters [2]. Many subsequent experiments measuring ionization potential (IP) and electron affinity (EA) of metal clusters [4–12] have put the ideas of the shell models on a firmer footing. An interesting consequence of shell models and magic clusters is the idea that certain atomic clusters can mimic chemical properties of elemental atoms. This originated as the idea of unified atom [13], but has subsequently led to superatoms. According the latest definition given by Castleman and Khanna, atomic clusters that posses useful properties, and retain their structural identity in assemblies, are called superatoms [14]. According to the ideas of the spherical shell model, Al_{13} cluster having 39 valence electrons is one electron short of a filled 2P shell, and therefore should behave like a halogen atom. This has been verified experimentally, and Al_{13} has been termed a superhalogen [15]. Al_{13}^-, being a 40-electron filled shell cluster, behaves like an inert gas atom as seen in its reactivity with oxygen [15,16]. Subsequently, Al_{14} and Al_{17}^- have also been found to behave as superatoms [17,18]. A large number assemblies of As-based superatoms have already been synthesized demonstrating that 'designer' materials with tunable electronic properties can be built using superatoms as building blocks [19].

Ideas of spherical shell models have been used to explain properties of 3d transition metal doped metal clusters also [20]. Photofragmentation mass spectra of the $TMAu_n^+$ clusters could be explained satisfactorily under the assumptions that Sc and Ti donated all their 3d and 4s electrons (3 and 4 respectively) to the valence pool, Cr–Co behaved as bivalent elements and Ni donated a single electron. Major drop in the abundance spectra of $ScAg_n^+$, $TiAg_n^+$ and VAg_n^+ clusters could also be explained by assuming that these TM atoms donate all their 3d and 4s electrons to the valence pool. In a recent series of theoretical works, we have used ideas of the spherical shell models to explain properties of TM doped alkali and alkaline earth clusters [21–25]. In the VNa_n and VCs_n series, VNa_8 and VCs_8 were found to be magic clusters even though they have 13 valence electrons each. In these clusters, five of the valence electrons occupy V 3d orbitals, giving it a half-filled configuration and a magnetic moment of 5 μ_B. The remaining eight electrons fill the 1S and 1P shell orbitals leading to enhanced stability [23]. In the

* Corresponding author. Tel.: +91 5322274307.
E-mail address: prasen@hri.res.in (P. Sen).

0301-0104/$ - see front matter © 2013 Elsevier B.V. All rights reserved.
http://dx.doi.org/10.1016/j.chemphys.2013.03.019

$TMMg_n$ and $TMCa_n$ series, $FeMg_8$ and $FeCa_8$ turned out to have enhanced stability, though they have 24 valence electrons each, not a shell filling number in the spherical shell models. In these clusters, crystal field effect causes a splitting of the 2D shell orbitals into sets of 4 and 1. In addition, there is an exchange splitting in the 2D shell orbitals which causes a sub-shell closing at 24 valence electrons leading to a spin moment of 4 μ_B, and at the same time giving $FeMg_8$ and $FeCa_8$ enhanced stability [24,25]. VCs_8, $FeMg_8$ and $FeCa_8$ were found to behave as superatoms that also posses magnetic moments. These were termed magnetic superatoms. Discovery of magnetic superatoms has opened up the possibility of tuning both electronic and magnetic properties of cluster assembled materials.

Given this background, it is natural to try to understand the electronic, structural and magnetic properties of TM-Sr clusters. Indeed, Medel et al. have recently studied $MnSr_n$ clusters and have identified $MnSr_9$ as a magnetic superatom [26]. Still, many questions about these clusters remain unanswered. The most interesting one is whether there are other TM-Sr clusters that behave as magnetic superatoms. A detailed understanding of the magnetic properties of the TM-Sr clusters for different TM atoms, and origin of magnetic coupling between these magnetic superatoms have also not been attempted so far. Another question of utmost practical importance is whether these superatom building blocks are stable in their reaction with oxygen. In this paper we try to gain understanding of these issues by studying structural, electronic and magnetic properties of all the 3d TM-doped Sr clusters. We start our explorations with $TMSr_8$ clusters, but are led to the $CrSr_n$ and $MnSr_n$ series for reasons that are discussed in the following. We propose $CrSr_9$ and $MnSr_{10}$ as magnetic superatom candidates with some caveat.

2. Theoretical methods

All our first principles electronic structure calculations were performed within the density functional theory (DFT) using two different approaches in different cases. In one approach, molecular orbitals (MO) were expressed as linear combinations of Gaussian type orbitals centered on the atomic nuclei. deMon2k [27] code was used for these calculations. Calculation of four-center integrals were avoided by a variational fitting of the Coulomb potential. The exchange–correlation effects were taken into account using the generalized gradient approximation (GGA) functional proposed by Perdew, Burke and Ernzerhof (PBE) [28] and were calculated through a numerical integration from the orbital density. For the Sr atom, a quasi-relativistic effective core potential (ECP) (with 28 electrons in the core) and basis set combination from Stuttgart–Dresden (QECP10|SD) distributed with deMon2K was used. This produced first and second ionization potentials of 5.71 and 11.10 eV for a Sr atom, which are in excellent agreement with experimental values of 5.70 and 11.03 eV respectively [29]. All electrons on the 3d TM atoms were treated explicitly using the double-ζ valence plus polarization basis sets optimized for GGA functionals by Calaminici et al. (DZVP-GGA) [30]. The auxiliary density was expanded in primitive Hermite Gaussians using the GEN-A2 auxiliary function set. This contains s, p, d, f and g auxiliary functions, and adapts automatically to the chosen orbital basis set [30]. A large number of initial structures were taken for each cluster. These initial structures were generated as follows. For $TMSr_n$ cluster, stable isomers of alkali and alkaline earth clusters for size $n+1$ were taken from our earlier works and the literature, and different metal atoms were replaced by a TM atom of interest. In addition, possible Sr cage structures encapsulating the TM atom were also taken. All possible spin states were considered for each initial structure, and all these clusters were fully optimized using a quasi-Newton method in the internal coordinates [31] without any symmetry constraints. To ensure that the optimized structures were local minima, harmonic frequencies were calculated for each one of them. If any structure turned out to have imaginary frequencies, it was re-optimized by distorting it along the unstable vibrational modes. Finding the global minimum structure of any cluster is known to be a difficult optimization problem because the number of local minima increases rapidly with the number of atoms in the cluster. However, for the small clusters we have considered here, we are reasonably confident to have found the global minimum.

In the second approach calculations were done using a planewave basis set with an energy cutoff of 350 eV within spin polarized DFT. The PBE GGA functional was used for the exchange–correlation functional in these calculations also. Brillouin zone integrations were performed using the Γ-point only. Ionic potentials were represented by Projector Augmented Wave (PAW) potential [32]. The clusters and their dimers were put in periodic boxes of such dimensions that the minimum distance between an atom in the calculation cell and the periodic image of any other atom was 10 Å. All the atoms were completely relaxed till the forces on each atom were less that 0.01 eV/Å. Using these parameters we obtained the same ground state structures and spin states for $CrSr_9$ and $MnSr_{10}$ clusters as in deMon2K. VASP code was used for these calculations [33]. When specifically not mentioned, we present deMon2K results.

3. Results and discussions

3.1. TM-Sr_8 clusters

Of various possibilities, we start with a single 3d TM doped Sr_8 clusters. One of the reasons behind this choice is our earlier finding that $FeMg_8$ and $FeCa_8$ are stable clusters that behave as magnetic superatoms. We have presented structure, spin multiplicity and bond lengths for all the $TMSr_8$ clusters in their ground states in the supplementary Figure S1. For Sc-Mn the $TMSr_8$ clusters have the square anti-prism structure as obtained for the $TMMg_8$ and $TMCa_8$, albeit with a larger alkali atom cage. The cage is distorted in case of VSr_8. $FeSr_8$, $CoSr_8$ and $NiSr_8$ have very different structures. They have bi-capped octahedron structure as obtained for $NiCa_8$. This is presumably because the late TM atoms are too small to form bonds with the Sr atoms if they are placed at the centre of a square anti-prism cage. However, in absence of compact symmetric structures, the MOs of these clusters do not have good resemblance to shell orbitals of definite angular momentum character, a point we discuss in some detail later. Before that we try to find the clusters in this series that have high stability. For this we calculate the hardness and the adiabatic spin excitation energy for these clusters. Hardness (η) of a cluster is defined as [34]

$$\eta = \frac{1}{2}\left(\frac{\partial \mu}{\partial N}\right)_v = \frac{1}{2}\left(\frac{\partial^2 E}{\partial N^2}\right)_v \quad (1)$$

μ is the chemical potential, E is the total energy and N is the number of electrons in the cluster. All the derivatives are to be taken at a constant external potential v. According to the maximum hardness principle [35] a molecule tries to maximize its hardness. In the finite difference approximation, the hardness can be approximated by

$$\eta \approx \frac{\mathrm{IP} - \mathrm{EA}}{2} \quad (2)$$

The IP and EA values can be calculated using Koopmans' theorem, in which case they are simply equal to the energies of the highest occupied (HOMO) and the lowest unoccupied molecular orbitals (LUMO) respectively. In this case hardness becomes half the

HOMO–LUMO gap. One can also find vertical IP and EA values by doing self consistent calculations for the cation and the anion respectively at the geometry of the neutral (ΔSCF method), and finding the energy difference between the neutral and the charged clusters. Adiabatic spin excitation energy (Δ_{spin}) of a cluster is defined as the energy difference between its ground state and the next higher energy spin multiplicity in their respective lowest energy structures. It indicates stability of the ground state of a cluster with respect to its excitation to the next higher energy spin state. Δ_{spin}, and η calculated using ΔSCF method for the $TMSr_8$ clusters are plotted in Fig. 1.

Fig. 1 shows that $TiSr_8$ has the largest η. This is because $TiSr_8$ is a 20 electron filled shell singlet with a $1S^2 1P^6 1D^{10} 2S^2$ electronic configuration. Hardness calculated using Koopmans' theorem also shows a maximum for $TiSr_8$. As already mentioned, the energy ordering of the orbitals in the spherical shell model is 1S|1P|1D|2S|1F|2P|... As we go across the 3d series in $TMSr_8$ clusters, the 2D shell orbitals, instead of the 1F or 2P orbitals, start getting occupied. 2D orbitals are stabilized due to the contribution of the TM d orbitals. The hardness goes down across the 3d series. $CoSr_8$ is an exception with a small peak in the hardness value. Δ_{spin} also decreases across the 3d series except for Mn and Co. Surprisingly, Δ_{spin} has a maximum value at $ScSr_8$. Why $ScSr_8$, a 19 electron cluster, has such a large Δ_{spin}, larger than that of $TiSr_8$, deserves an explanation. To aid this, MO energy level diagrams and isosurfaces for the $ScSr_8$ and $TiSr_8$ clusters are shown in Fig. 2. $ScSr_8$ is a doublet with an electronic configuration $1S^2 1P^6 1D^9 2S^2$. The $1D_Z^2$ orbital in the β-channel is split off to a higher energy due to crystal-field effect as discussed in our earlier works [24,25]. To excite this cluster to a quartet spin state one has to excite an electron from the highest occupied degenerate 1D orbitals in the β-channel to the LUMO in the α-channel. Within the 'frozen orbital' approximation, the energy required for the process is ~1 eV. On the other hand, to excite $TiSr_8$ to a triplet state one has to excite one of the electrons from the HOMO to the LUMO. The required energy for this, within 'frozen orbital' approximation, is simply the HOMO–LUMO gap of the cluster, which is 0.76 eV. The actual Δ_{spin} values obtained after self-consistent calculations of the spin-excited states are slightly different from these numbers. $ScSr_8$ has a larger Δ_{spin} nevertheless. In addition to hardness, electrophilicity index (ω) also indicates reactivity of a cluster. According to the minimum electrophilicity principle, a chemical species tries to minimize its electrophilicity index [36]. Stability of Al-based superatoms and other molecules have been understood using the maximum hardness and minimum electrophilicity principles [36]. Electrophilicity index (ω) is defined as

$$\omega = \frac{\chi^2}{2\eta} \tag{3}$$

where χ is the electronegativity. χ is equal to negative of the chemical potential (μ) and can be written as $\chi = -\mu = (IP + EA)/2$. ω does

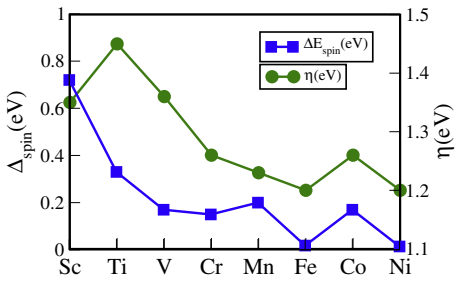

Fig. 1. Hardness and adiabatic spin excitation energies of all 3d TM doped $TMSr_8$ clusters.

have a minimum for $TiSr_8$ indicating its enhanced stability. Electronegativity, hardness and electrophilicity index values of all the clusters studied here are given in the supplementary information.

Although $CoSr_8$ shows enhanced stability compared to its neighbors in Fig. 1, lack of a compact structure makes its interpretation in terms of electronic shell models difficult. The frontier orbitals of $CoSr_8$ do not resemble shell orbitals of definite angular momentum character. Moreover, it is not an attractive candidate as a magnetic superatom because of its low-spin state. Low-spin state also makes $ScSr_8$ unattractive from the point of view of magnetic superatom, though it has large gap and Δ_{spin}.

$FeSr_8$ and $NiSr_8$ are found to have triplet ground states in bi-capped octahedral structure. These two clusters also have close-lying spin isomers and so have very small Δ_{spin} values. Therefore, we looked at the higher energy spin isomers more closely. It turns out that the spin-excited state of the $FeSr_8$ cluster is a quintet in a square anti-prism structure. Having a more compact and symmetric structure, its MOs bear closer resemblance to the shell orbitals. To illustrate the point MO energy level diagrams for the two isomers of $FeSr_8$ are given in the supplementary Figure S2. The 2S orbitals in $^5FeSr_8$ are nearly spherical, which is not the case in $^3FeSr_8$. We found it difficult to assign any definite angular momentum character to the HOMO-1 and the orbital just below the three 1P orbitals in the α-channel in $^3FeSr_8$. The quintet excited state $^5FeSr_8$ has exactly the same electronic configuration as $^5FeMg_8$ and $^5FeCa_8$ [24,25]. $NiSr_8$, on the other hand, has an immediate higher energy state that is a singlet in the same bi-capped octahedron structure.

A full understanding of the electronic and magnetic properties of these clusters also requires an understanding of the origin of magnetic moments. A Mulliken population analysis in deMon2K shows that in the Sc, V, Cr, Mn and Fe doped clusters, most of the moment is on the TM atoms. However, there are small magnetic moments on all the Sr atoms. In the V and Cr doped clusters these add up to a contribution that is comparable to (within a factor of ~1/2) the moment on the central TM atoms. Except in $FeSr_8$, the Sr moments are oriented opposite to the moment on the TM atom. In $CrSr_8$, the moment on the Cr atom is 3.9 μ_B, while each Sr atom has ~0.24 μ_B oriented in the opposite direction. In $MnSr_8$, the Mn atom has a moment of 3.46 μ_B, while the moment on each of the Sr atoms is only $\leqslant$0.06 μ_B adding up to 0.46 μ_B, oriented opposite to the Mn moment. $CoSr_8$ and $NiSr_8$ are qualitatively different from the other clusters. Most of the moment in these is on the Sr atoms. In $CoSr_8$, the moment on the Co atom is only 0.08 μ_B, while four of the Sr atoms have ~0.17 μ_B each. In $NiSr_8$ also, the Ni atom has a tiny moment (0.009 μ_B), and almost the entire moment is on the Sr atoms. The highest moment on the Sr atoms is 0.32 μ_B. Thus all the TM atoms (except Ti) polarize the electron gas spread over the Sr cage in these clusters. The situation in $^3NiSr_8$ where there are spin moments on the Sr atoms while the moment on the Ni atoms is almost zero, is somewhat similar to the recently discovered high-spin ground state of the icosahedral Cs_{13} cluster [37].

3.2. $CrSr_n$ and $MnSr_n$ clusters

Having explored the $TMSr_8$ series we now ask if there are TM-Sr clusters at other sizes that have enhanced stability and large magnetic moment, and whether they can be candidates for magnetic superatoms. At this point it is important to recount that specific shape and size of a cluster can lead to sub-shell filling at electron numbers not predicted by perfectly spherical models. Therefore, only after first-principles calculations are done and the ground state structures identified, can one understand why a particular cluster turns out to have enhanced stability. As mentioned before, $FeMg_8$ and $FeCa_8$ are examples of this. These two clusters have

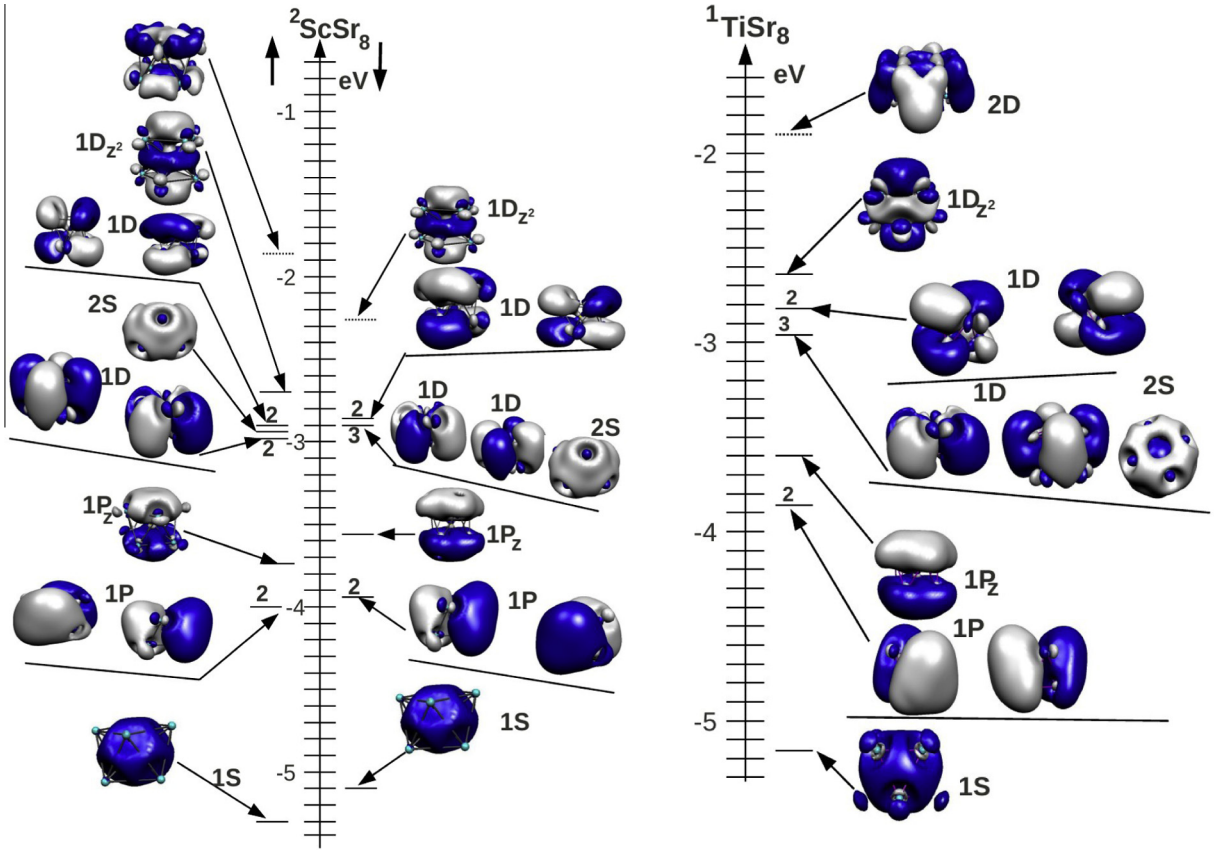

Fig. 2. MO energy level diagrams and isosurface plots for the $ScSr_8$ and $TiSr_8$ clusters in their ground states. Correspondence with the shell orbitals are indicated beside each MO. Degeneracies are also marked.

enhanced stability, though they have 24 valence electrons each. With this hindsight, we ask if other 24-electron clusters in the TM-Sr series could also attain enhanced stability. A hint for this came from the MO energy level diagram of the $CrSr_8$ cluster that we show in Fig. 3(a). $CrSr_8$ is a 22-electron cluster and has an electronic configuration of $1S^2 1P^6 1D^{10} 2S^2 2D_\alpha^2$. The HOMO of $CrSr_8$ consists of doubly degenerate 2D orbitals in the α channel. Two degenerate 2D orbitals form the LUMO in the same spin channel. This suggests that if another Sr atom is added, the two valence electrons coming from it are likely to go in the α channel, and this 24-electron cluster may have high stability just like $FeMg_8$.

To explore this exciting possibility, we studied $CrSr_n$ clusters over the size range $n = 4$–12. Ground state structures, spin multiplicities and bond lengths of all these clusters are given in the supplementary Figure S3(a). The Cr atom gets completely embedded in a Sr cage for the first time at $n = 6$. $CrSr_7$ has a pentagonal bi-pyramid structure. $CrSr_9$ and $CrSr_{10}$ are capped and bi-capped square anti-prisms. $CrSr_{12}$ has a structure which is obtained by capping two triangular faces of the $CrSr_{10}$ motif. The hardness values and second order energy differences of these clusters with increasing number of Sr atoms are shown in Fig. 4(a). Second order energy difference is defined as

$$\Delta_n^2 = E(TMSr_{n+1}) + E(TMSr_{n-1}) - 2E(TMSr_n) \quad (4)$$

Δ_n^2 measures relative thermodynamic stability of the $TMSr_n$ cluster with respect to both $TMSr_{n-1}$ and $TMSr_{n+1}$ [3]. Both η and Δ_2 have peaks at size nine indicating enhanced stability of $CrSr_9$. Δ_2 also has a distinct peak at size indicating its thermodynamic stability compared to neighboring sizes. However, $CrSr_6$ does not have a peak in the hardness.

Further insights into the enhanced stability of $CrSr_9$ can be obtained by studying its MO energy level diagram that is shown in Fig. 3(b). Interestingly, our conjecture that the two additional electrons (relative to $CrSr_8$) will go into the 2D orbitals in the α-channel turns out to be true. $CrSr_9$ has an electronic configuration $1S^2 1P^6 1D^{10} 2S^2 2D_\alpha^4$ giving it a spin moment of 4 μ_B. The remaining 2D orbital in the α-channel is split-off to a higher energy due to crystal-field effect, giving a large HOMO–LUMO gap and a large hardness. There is also a large exchange splitting in the 2D orbitals. The next higher energy orbitals above the 2D orbitals in the α-channel and the 1D orbitals in the β-channel are of $2P_z$ character. This is also due to the crystal field effect. Because of the elongated shape of the cluster in one direction (truncated prolate spheroid), the $2P_z$ shell orbitals are stabilized compared to the other P orbitals. $CrSr_{11}$ also shows a large HOMO–LUMO gap and hardness though it does not have a peak in Δ^2. It has a tri-capped anti-prism structure. Again a non-compact structure of this cluster leads to a poor resemblance of its MOs to the shell orbitals. Therefore, we do not attempt to explain the large gap in terms of these models. ω calculated using Koopmans' theorem also shows minima for $CrSr_9$ and $CrSr_{11}$. ω within ΔSCF, however, does not have a minimum at $CrSr_9$, rather it shows minima for $CrSr_6$ and $CrSr_{11}$. Thus the signal from calculated ω values is not entirely clear. It has been shown that $PbNa_6$ cluster has enhanced stability due to a compact high symmetry octahedral structure and an electronic shell filling arising from a modified shell model which has an attractive potential at the center due to the presence of the Pb atom [39]. We believe that shell filling does not happen in $CrSr_6$ because it has a lower HOMO–LUMO gap than $CrSr_5$. The absence of a local maximum in the HOMO–LUMO gap and hardness for $CrSr_6$ indicates that its stability most likely originates from a compact geometric struc-

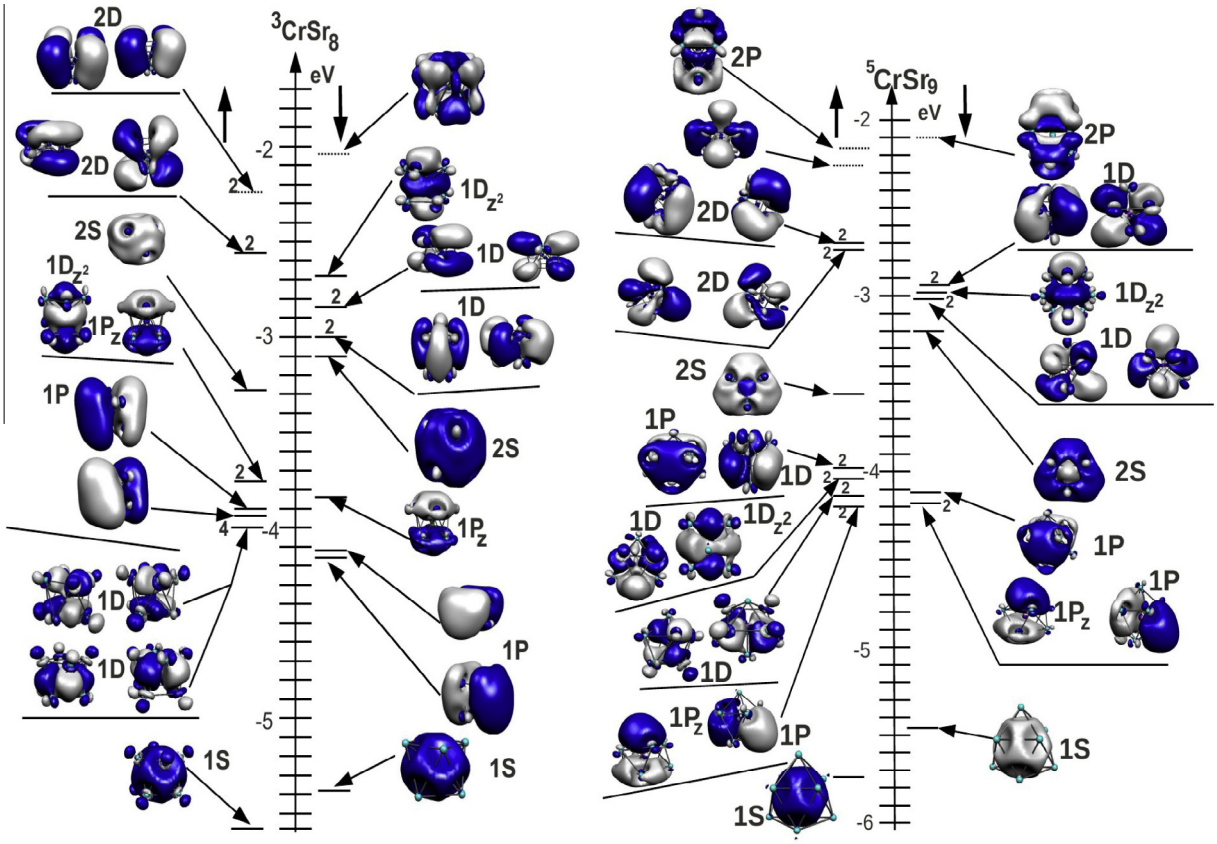

Fig. 3. MO energy level diagrams and isosurface plots for the $CrSr_8$ and $CrSr_9$ clusters in their ground states. Correspondence with the shell orbitals are indicated beside each MO. Degeneracies are also marked.

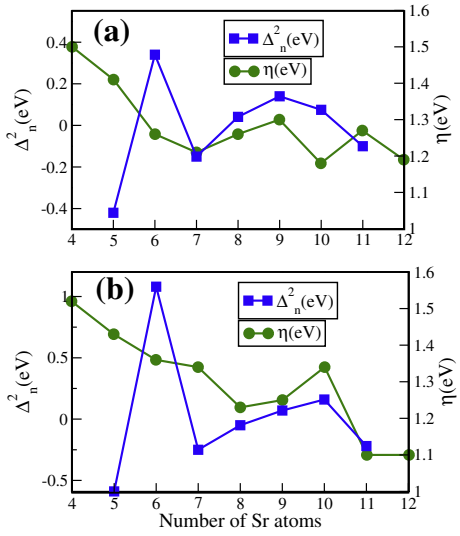

Fig. 4. Hardness and the second order energy difference Δ^2_n for the (a) $CrSr_n$ and (b) $MnSr_n$ clusters as a function of the number of Sr atoms n.

ture. The situation is similar to that of Ti-alkali [21] and TM-Ge [38] clusters. Calculated electronegativity, hardness and electrophilicity index values of all the $CrSr_n$ clusters are given in the supplementary table S2.

Next we focus on the Mn-Sr clusters. In particular, $MnSr_9$ cluster has one electron more than $CrSr_9$, and has a $1S^21P^61D^{10}2S^22D_z^5$ electronic configuration [26]. A half-filled 2D electronic configuration may lead to large HOMO–LUMO gap and hence large hardness and enhanced stability. Surprisingly, Medel et al. [26] found $MnSr_{10}$ to have the highest HOMO–LUMO gap, though, $MnSr_9$ turned out to have the highest Sr addition energy. They went onto identify $MnSr_9$ as a magnetic superatom. To understand this apparent dichotomy, we decided to have another look at the $MnSr_n$ clusters. Ground state structures for these clusters from $n = 9$–12 are shown in the supplementary Figure S3(b). Since the structures for $n = 6$–8 are essentially what is reported in Ref. [26], and are not central to what follows, we have not shown them. $MnSr_9$ and $MnSr_{10}$ have the same structures as $CrSr_9$ and $CrSr_{10}$. The structure of $MnSr_{11}$ is obtained by capping three side triangular faces of the $MnSr_8$ anti-prism motif. Similarly, $MnSr_{12}$ has a ground state structure that can be viewed as four Sr atoms capping the side triangular faces of the $MnSr_8$ anti-prism motif. We plot the hardness and the second order energy difference the $MnSr_n$ clusters in Fig. 4(b). We would like to point out that the Sr addition energy reported in Ref. [26] reflects stability of $MnSr_n$ relative to $MnSr_{n-1}$, whereas the second order energy difference reflects its stability relative to both $MnSr_{n-1}$ and $MnSr_{n+1}$. Which of these is more relevant will depend on the experimental conditions. For example, in a seeded supersonic nozzle source, where clusters are produced at their evaporation temperatures and the final step leading to stabilization is evaporation of one or more atoms, Δ^2 will be more relevant to defining stability. On the other hand, for cold clusters produced in a gas-aggregation cluster source, where cluster growth involves single-atom addition at a time, Sr addition energy will be more relevant [3]. Δ^2 has a distinct peak for $MnSr_6$ just as for $CrSr_6$ without any associated peak in the hardness. This enhanced thermodynamic stability of $MnSr_6$ can also be attributed to its compact octahedral structure. More interestingly, $MnSr_{10}$ shows a local maximum in both hardness and Δ^2. To explain the observed

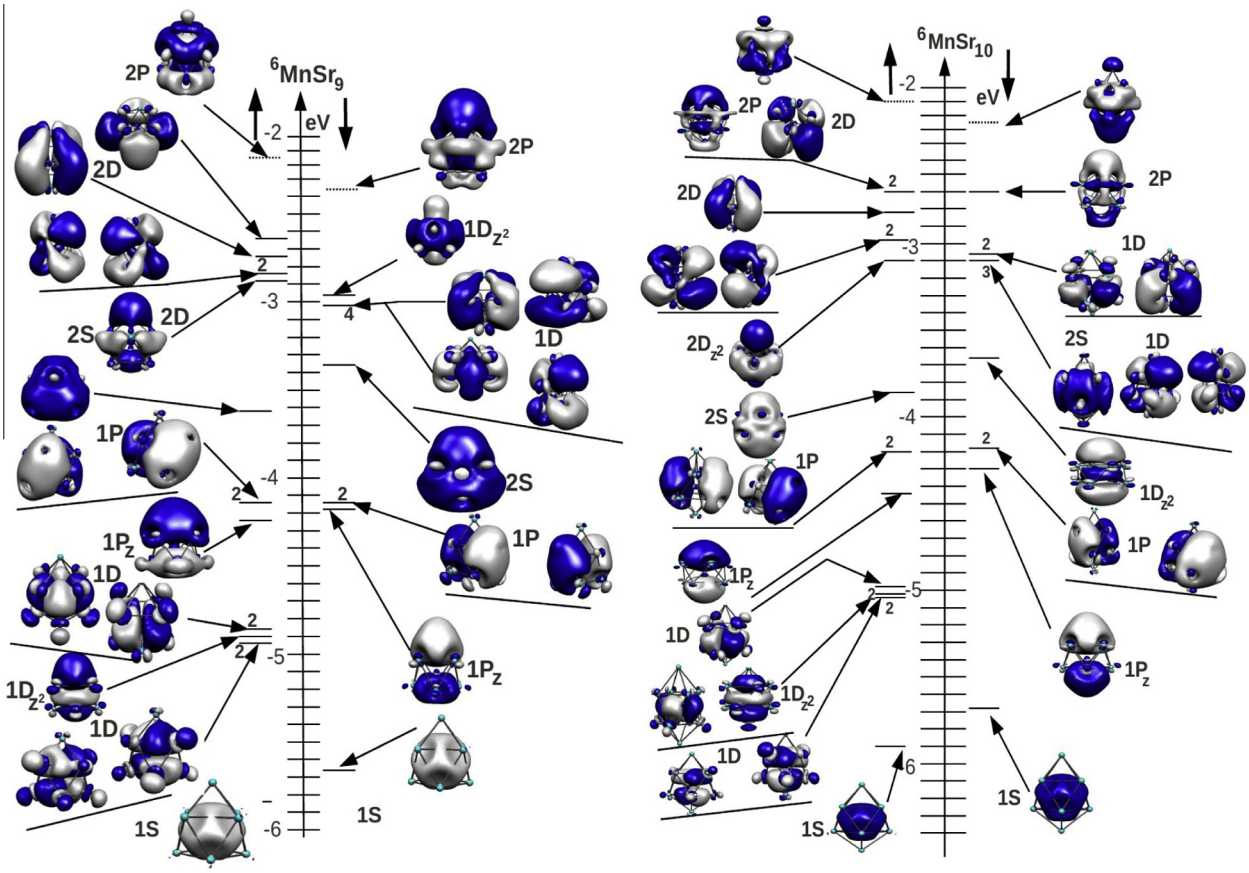

Fig. 5. MO energy level diagrams and isosurface plots for the $MnSr_9$ and $MnSr_{10}$ clusters in their ground states. Correspondence with the shell orbitals are indicated beside each MO. Degeneracies are also marked.

stability of $MnSr_{10}$ we show the MO energy level diagrams of both $MnSr_9$ and $MnSr_{10}$ in Fig. 5. The $MnSr_9$ has a $1S^2 1P^6 1D^{10} 2S^2 2D^5_\alpha$ configuration as already shown in Ref. [26]. This also has a capped square anti-prism structure which stabilizes the $2P_z$ orbitals. Because of half filled 2D states, $MnSr_9$ has a HOMO–LUMO gap of 0.51 eV in the α channel. However, the LUMO in the β channel, which is a $2P_z$ orbital, is slightly lower in energy than the LUMO in the α channel, and the overall gap (0.32 eV) is smaller than that of $CrSr_9$ (0.46 eV). Something interesting happens as another Sr atom is added to $MnSr_9$. This Sr atom caps the remaining square face of $MnSr_9$ leading to a bi-capped square anti-prism structure for $MnSr_{10}$. This further elongated shape of the cluster in one direction produces a crystal field that stabilizes the P_z orbitals even further. The P_z orbital becomes occupied in both the spin channels, and it becomes degenerate with the highest occupied 2D orbital in the α channel. Stabilization of the $2P_z$ orbitals[1] leads to sub-shell filling at this size leading to a large HOMO–LUMO gap (0.45 eV) and enhanced stability of $MnSr_{10}$. Electrophilicity index also has a minimum at $MnSr_{10}$ as shown in the supplementary table S3.

Spin moments on the $CrSr_9$, $MnSr_9$ and $MnSr_{10}$ clusters have the same origin as $TMSr_8$ clusters. Mulliken population analysis shows that in $CrSr_9$, the Cr atom has a moment of 4.34 μ_B, and most of the Sr atoms have moments aligned opposite to this so that the net moment is 4 μ_B. In $MnSr_9$ and $MnSr_{10}$, the moments on the Mn atom are 3.74 and 3.95 μ_B respectively. The moments on the Sr atoms are aligned parallel to the Mn moments in these clusters, and they add up to 5 μ_B in both cases. The electron gas on the Sr cage is polarized in these clusters also.

[1] These MOs have one radial node and hence are of 2P character and not 1F.

3.3. Assemblies of $CrSr_9$ and $MnSr_{10}$

Having demonstrated that $CrSr_9$ and $MnSr_{10}$ are stable clusters with high magnetic moments, we now study their behavior in assemblies. A major practical difficulty in building assemblies of clusters is that they have a tendency to coalesce [14]. For example, in our earlier work it was found that two VNa_8 units coalesce and lose their structural identities. VCs_8 units, however, retain their identities [23]. To address this question in the present case, we studied dimers of $CrSr_9$ and $MnSr_{10}$ clusters through spin polarized DFT calculations using the VASP code. Two cluster units were brought close to each other from different directions and in different orientations. In all the cases we studied both parallel and anti-parallel alignments of the TM spins. In all the cases the individual cluster units retained their structural identity (apart from some minor distortions). Two $CrSr_9$ units with their spins aligned parallel to each other and having a total moment of 8 μ_B turned out to have the lowest energy. In this state the dimer has a binding energy (BE) of 2.54 eV relative to the isolated $CrSr_9$ units. The distance between two Cr atoms is 6.82 Å. An anti-parallel alignment of the Cr spins in the two units is found to be 0.37 eV higher. The Cr–Cr distance in this case is 8.11 Å. In case of $MnSr_{10}$ also, a parallel arrangement of the spins on the two clusters with a total moment of 6 μ_B, and a BE of 2.51 eV turned out to have the lowest energy. The Mn–Mn distance in this structure is found to be 6.97 Å. A dimer with anti-parallel alignment of the Mn spins is 0.34 eV higher, and the Mn–Mn distance in this structure is 6.92 Å. Structures of these dimers are shown in the supplementary Figure S4. Thus both $CrSr_9$ and $MnSr_{10}$ behave as magnetic superatoms. As has been shown before, such superatoms can play useful role as spin filter [40] and in other applications.

A sizable energy difference between the parallel and anti-parallel alignments of the spins on the TM atoms in the dimers indicate a substantial coupling between them. Similar energy difference was found in the dimers of VCs_8 clusters also. So far, no attempt has been made to understand the mechanism of the coupling between these magnetic superatoms. Here we attempt to offer a qualitative understanding of this phenomenon. As we have already mentioned, the moment on the TM atoms polarize the electron gas in the cluster leading to moments on the Sr atoms. The orientation of this polarization bears a definite relation to the moment on the TM atoms in the Cr and Mn doped clusters: it is anti-parallel to the Cr moment in $CrSr_9$, and parallel to the Mn moment in $MnSr_{10}$. In the dimers of these clusters, there are, in a way, two groups of Sr atoms intervening between the two TM atoms, one group belonging to each cluster originally. When both the TM atoms have their spins parallel to each other, all the intervening Sr atoms have their spins oriented in the same direction, that is, the entire electron gas is polarized in a particular direction. When the TM spins are oriented anti-parallel, they tend to orient the spins on different groups of intervening Sr atoms in opposite directions creating a 'frustration' in the system, and increasing the energy. In other words, the interaction between the TM spins seems to be mediated by the polarization of the electron gas spread over the Sr cages.

3.4. Reactivity with oxygen

While the previous results are encouraging, another issue of practical relevance is the reactivity of these superatoms towards molecular oxygen. Although we have shown that $CrSr_9$ and $MnSr_{10}$ have large HOMO–LUMO gaps and hardness values compared to the neighboring sizes, the values of the gaps are ~0.45 eV. For a comparison, this is much smaller than 1.69 eV, the HOMO–LUMO gap of Al_7C^- which shows no reactivity towards molecular oxygen [18]. Besides its HOMO–LUMO gap and hardness, the spin excitation energy of a cluster also plays a decisive role in its reactivity towards oxygen. Detailed theoretical and experimental work on pure and hydrogenated aluminum cluster anions have proved that clusters having unpaired spins or small singlet–triplet spin excitation energies are readily etched away by oxygen, while those having large spin excitation energies are not reactive [41]. Clusters having unpaired spins or small spin excitation energy can easily transfer electrons to the anti-bonding LUMO in the minority spin channel of the O_2 molecule facilitating its dissociation. Clusters that were etched away easily by oxygen were also found to dissociate O_2 without a barrier in DFT calculations. The O_2 molecule, after dissociation, had large binding energies to these clusters. Both $CrSr_9$ and $MnSr_{10}$ having unpaired spins, it is imperative to see if they also dissociate O_2 without a barrier. Therefore we consider the most likely reactions of these two clusters with a O_2 molecule:

$$^5CrSr_9 + {}^3O_2 \rightarrow {}^3CrSr_7 + 2\,{}^1SrO \quad \text{and}$$

$$^6MnSr_{10} + {}^3O_2 \rightarrow {}^4MnSr_8 + 2\,{}^1SrO$$

Both reactions conserve total spin. First we ask whether the reactions are energetically favored. We calculated total energies of all the species in their respective spin states shown in the above equations. It turns out that the first reaction is favorable by 0.79 eV, and the second one is favorable by 1.00 eV. Energetics being favorable, the next question is the kinetics of the O_2 bond breaking. To understand whether there is a barrier to this process, we brought an O_2 molecule close to each of these clusters from different directions and in different orientations. Except in the case when the O_2 molecule approaches the apical Sr atoms vertically, the O–O bond dissociates spontaneously during structure relaxation. In the energetically most favorable structures for both the clusters, the two O atoms cap two triangular faces. The BE of the O_2 molecule to $CrSr_9$ and $MnSr_{10}$ are quite large, and are 9.93 and 9.82 eV respectively. These may be compared to the BE of 8.65 eV of O_2 to Al_5^-, a cluster which is easily etched away [41]. We define the BE of the O_2 molecule to these clusters as

$$BE = E(^{M}TMSr_n) + E(^3O_2) - E(^{M-2}TMSr_nO_2)$$

This indicates that these clusters will likely be etched away by molecular oxygen. Incidentally, our calculations show that O_2 dissociates on $MnSr_9$ also without a barrier.

3.5. Final prospects

This leads us to the final question whether these superatoms will be useful in building cluster assembled materials or other applications. All assemblies of As-based clusters synthesized so far have been done through the chemical route [19]. In this process there are no possibilities of individual cluster units reacting with oxygen and getting etched away. Therefore, if assemblies of TM-Sr superatoms can be synthesized through the chemical route, reactivity of individual clusters with O_2 will not be a hindrance. However, for other applications in which individual clusters have to be manipulated (such as depositing size selected clusters on a substrate) one has to avoid their contact with O_2. Whether any of this is possible or useful will finally have to be answered by experiments. We believe that the present theoretical work will motivate serious experimental efforts in this direction.

4. Conclusions

A detailed study of the structural, electronic and magnetic properties of 3d TM doped Sr clusters have been performed using DFT methods. Our calculations reveal that in the $TMSr_8$ series, $TiSr_8$ being a filled shell singlet, has the largest hardness. Strangely, $ScSr_8$ has the largest spin excitation energy. This can be understood by looking at the details of the spin excitation process involved. Except in $CoSr_8$ and $NiSr_8$, most of the moment is found on the TM atoms within a Mulliken population analysis. In these two clusters, the Sr atoms carry most of the moment. $CoSr_8$ is found to have a local peak in the hardness and the spin excitation energy. However, in absence of a compact symmetric structure, the correspondence of its MOs with the orbitals of a spherical shell model is rather poor. Moreover, a small moment makes it unattractive from the point of view of magnetic superatoms. Our search for stable clusters at other sizes led to the $CrSr_n$ and $MnSr_n$ series which we studied for $n = 4$–12. $CrSr_9$ and $MnSr_{10}$ turned out to have enhanced kinetic and thermodynamic stabilities. Both these clusters were found to behave as magnetic superatoms in their assemblies. However, these and $MnSr_9$ were found to be reactive towards molecular oxygen. This puts practical constraints on the conditions under which these superatoms can be used in applications.

Acknowledgment

All the calculations were performed at the cluster computing facility at HRI, Allahabad (http://cluster.hri.res.in).

Appendix A. Supplementary data

Supplementary data associated with this article can be found, in the online version, at http://dx.doi.org/10.1016/j.chemphys.2013.03.019.

References

[1] W. Ekardt, Phys. Rev. B 29 (1984) 1558.
[2] W.D. Knight, K. Clemenger, W.A. de Heer, W.A. Saunders, M.Y. Chou, M.L. Cohen, Phys. Rev. Lett. 52 (1984) 2141.
[3] W.A. de Heer, Rev. Mod. Phys. 65 (1993) 611.
[4] E. Benichou, A.R. Allouche, M. Aubert-Frecon, R. Antonie, M. Broyer, P. Dugourd, D. Rayane, Chem. Phys. Lett. 290 (1998) 171.
[5] P. Dugourd, D. Rayane, P. Labastie, B. Vezin, J. Chevaleyre, M. Broyer, Chem. Phys. Lett. 197 (1992) 433.
[6] M.M. Kappes, M. Schär, U. Röthlisberger, C. Yeretzian, E. Schumacher, Phys. Lett. 143 (1988) 251.
[7] W.A. Saunders, K. Clemenger, W.A. de Heer, W.D. Knight, Phys. Rev. B 32 (1985) 1366.
[8] K.E. Schriver, J.L. Prsson, E.C. Honea, R.L. Whetten, Phys. Rev. Lett. 64 (1990) 2539.
[9] C.L. Pettiette, S.H. Yang, M.J. Craycraft, J. Conceiaco, R.T. Laaksonen, O. Cheshnovsky, R.E. Smalley, J. Chem. Phys. 88 (1988) 5377.
[10] G. Gantefor, M. Gaussa, K.H. Meiwes-Broer, H.O. Lutz, Z. Phys. D 9 (1988) 253.
[11] G. Gantefor, M. Gaussa, K.H. Meiwes-Broer, H.O. Lutz, Faraday Diss. Chem. Soc. 86 (1988) 197.
[12] K.J. Taylor, C.L. Pettiette-Hall, O. Cheshnovsky, R.E. Smalley, J. Chem. Phys. 96 (1992) 3319.
[13] P. Jena, S.N. Khanna, B. Rao, Mat. Sc. For. 232 (1996) 1.
[14] A.W. Castleman Jr, S.N. Khanna, J. Phys. Chem. C 113 (2009) 2664.
[15] D.E. Bergeron, A.W. Castleman Jr, T. Morisato, S.N. Khanna, Science 304 (2004) 84.
[16] R.E. Leuchtner, A.C. Harms, A.W. Castleman Jr., J. Chem. Phys. 91 (1989) 2753.
[17] D.E. Bergeron, P.J. Roach, A.W. Castleman Jr., N.O. Jones, S.N. Khanna, Science 307 (2005) 231.
[18] J.U. Reveles, S.N. Khanna, P.J. Roach, A.W. Castleman Jr., PNAS 103 (2007) 18405.
[19] S.A. Claridge, A.W. Castleman, S.N. Khanna, C.B. Murray, A. Sen, P.S. Weiss, ACS Nano 3 (2009) 244;
M. Qian, A.C. Reber, A. Ugrinov, N.K. Chaki, S. Mandal, H.M. Saavedra, S.N. Khanna, A. Sen, P.S. Weiss, ACS Nano 4 (2010) 235;
N.K. Chaki, S. Mandal, A.C. Reber, M. Qian, H.M. Saavedra, P.S. Weiss, S.N. Khanna, A. Sen, ACS Nano 4 (2010) 5813;
A.C. Reber, S. Mandal, M. Qian, H.M. Saavedra, P.S. Weiss, S.N. Khanna, A. Sen, J. Phys. Chem. C 116 (2012) 10207.
[20] E. Janssens, H. Tanaka, S. Neukermans, R.E. Silverans, P. Lievens, Phys. Rev. B 69 (2004) 085402;
E. Janssens, S. Neukermans, H.M.T. Nguyen, M.T. Nguyen, P. Lievens, Phys. Rev. Lett. 94 (2005) 113401;
S. Neukermans, E. Janssens, H. Tanaka, R.E. Silverans, P. Lievens, Phys. Rev. Lett. 90 (2003) 033401;
X.-J. Hou, E. Janssens, P. Lievens, M.T. Nguyen, Chem. Phys. 330 (2006) 365.
[21] J.U. Reveles, P. Sen, K. Pradhan, D.R. Roy, S.N. Khanna, J. Phys. Chem. C 114 (2010) 10739.
[22] K. Pradhan, J.U. Reveles, P. Sen, S.N. Khanna, J. Chem. Phys. 132 (2010) 124302.
[23] J.U. Reveles, P.A. Clayborne, A.C. Reber, S.N. Khanna, K. Pradhan, P. Sen, M.R. Pederson, Nat. Chem. 1 (2009) 310.
[24] V.M. Medel, J.U. Reveles, S.N. Khanna, V. Chauhan, P. Sen, A.W. Castleman Jr, PNAS 108 (2011) 10062.
[25] V. Chauhan, V.M. Medel, J.U. Reveles, S.N. Khanna, P. Sen, Chem. Phys. Lett. 528 (2012) 39.
[26] V.M. Medel, J.U. Reveles, S.N. Khanna, J. Appl. Phys. 112 (2012) 064313.
[27] A.M. Köster, P. Calaminici, M.E. Casida, R. Flores-Moreno, G. Geudtner, A. Goursot, T. Heine, A. Ipatov, F. Janetzko, J.M. del Campo, S. Patchkovskii, J.U. Reveles, D.R. Salahub, A. Vela, deMon2k, V. 2.3.6, The deMon Developers Community, Cinvestav, México, 2006; available at <www.deMon-software.com>.
[28] J.P. Perdew, K. Burke, M. Ernzerhof, Phys. Rev. Lett. 77 (1996) 3865.
[29] N. Boutassetta, A.R. Allouche, M. Aubert-Frécon, Phys. Rev. A 53 (1996) 3845.
[30] P. Calaminici, F. Janetzko, A.M. Köster, R. Mejia-Olvera, B.J. Zúñiga-Gutierrez, Chem. Phys. 126 (2007) 044108.
[31] J.U. Reveles, A.M. Köster, J. Comp. Chem. 25 (2004) 1109.
[32] P.E. Blöchl, Phys. Rev. B 50 (1994) 17953.
[33] G. Kresse, J. Hafner, Phys. Rev. B 47 (1993) 558(49), 1994, 14251. G. Kresse, Thesis, Technische Universität at Wien 1993.;
G. Kresse, J. Furthmüller, Comput. Mat. Sci. 6 (1996) 15;
G. Kresse, J. Furthmüller, Phys. Rev. B 54 (1996) 11169.
[34] R.G. Parr, W. Yang, Density Functional Theory of Atoms and Molecules, Oxford University Press, New York, 1989.
[35] P.K. Chattaraj, U. Sarkar, D.R. Roy, Chem. Rev. 106 (2006) 2065;
R.G. Parr, P.K. Chattaraj, J. Am. Chem. Soc. 113 (1991) 1854.
[36] E. Chamorro, P.K. Chattaraj, P. Fuentelba, J. Phys. Chem. A 107 (2003) 7068;
P.K. Chattaraj, S. Giri, J. Phys. Chem. A 111 (2007) 11116;
R. Parthasarathi, M. Elango, V. Subramanian, P.K. Chattaraj, Theo. Chem. Acc. 113 (2005) 257.
[37] A. Aguado, J. Phys. Chem. C 116 (2012) 6841.
[38] D. Bandyopadhyay, P. Kaur, P. Sen, J. Phys. Chem. A 114 (2010) 12986.
[39] L.C. Balbás, J.L. Martins, Phys. Rev. B 54 (1996) 2937.
[40] H. He, R. Pandey, J.U. Reveles, S.N. Khanna, S. Karna, Appl. Phys. Lett. 95 (2009) 192104.
[41] A.C. Reber, S.N. Khanna, P.J. Roach, W.H. Woodward, A.W. Castleman Jr., JACS 129 (2007) 16098.